IEEE Access
Multidisciplinary | Rapid Review | Open Access Journal

Received December 11, 2020, accepted January 15, 2021, date of publication January 22, 2021, date of current version February 10, 2021.

Digital Object Identifier 10.1109/ACCESS.2021.3053596

Active Fault Tolerant Control System Design for Hydraulic Manipulator With Internal Leakage Faults Based on Disturbance Observer and Online Adaptive Identification

HOANG VU DAO[1], DUC THIEN TRAN[2], (Member, IEEE), AND KYOUNG KWAN AHN[3], (Senior Member, IEEE)

[1]Graduate School of Mechanical Engineering, University of Ulsan, Ulsan 44610, South Korea
[2]Automatic Control Department, Ho Chi Minh City University of Technology and Education, Ho Chi Minh City 700000, Vietnam
[3]School of Mechanical Engineering, University of Ulsan, Ulsan 44610, South Korea

Corresponding author: Kyoung Kwan Ahn (kkahn@ulsan.ac.kr)

This work was supported by the Basic Science Program through the National Research Foundation of Korea (NRF) funded by the Ministry of Science and ICT, South Korea, under Grant NRF 2020R1A2B5B03001480.

ABSTRACT In this paper, an active fault-tolerant control (FTC) system design is proposed for an n-degree-of-freedom (n-DOF) hydraulic manipulator with internal leakage faults and mismatched/matched lumped disturbances. A pair of matched and mismatched disturbance observers (DOBs) is proposed to simultaneously estimate and compensate for the effects of matched/mismatched disturbances on the control system in healthy conditions. The fault detection is achieved when the estimated matched disturbance is larger than a threshold. After that, a novel control reconfiguration law is designed to switch from a normal controller to a fault-tolerant controller with an online identification algorithm based on an adaptive mechanism. The proposed active FTC guarantees the position tracking performance in not only single-fault but also simultaneous-faults conditions. Moreover, the problem of uniting disturbance-observer-based control for external disturbance and adaptive control for parametric uncertainty is solved in a novel approach. Simulation results are conducted in a two-degree-of-freedom hydraulic leg prototype, which verifies the effectiveness of the proposed method.

INDEX TERMS Fault-tolerant control (FTC), disturbance observer (DOB), online identification, hydraulic manipulator, internal leakage fault.

I. INTRODUCTION

Electrohydraulic servomechanism has a high-power-to-weight ratio and large force/torque output compared to servo systems driven by pneumatic or electrical actuators [1]. As a result, electrohydraulic systems have been widely applied in industrial automation applications and/or military applications including active suspensions [2], [3], rolling mills [4], aircraft actuators [5], robot manipulators [6]–[10], and construction machines [11]. However, the performance of the servo system driven by electrohydraulic actuators usually is strongly affected by highly nonlinearities, modeling uncertainties (e.g., Bulk modulus, friction, and leakage), and external disturbance (e.g., load variations) [12], [13]. To deal with these problems, several approaches have been proposed.

The associate editor coordinating the review of this manuscript and approving it for publication was Moussa Boukhnifer.

Assuming that exact model parameters are available, the highly nonlinear behavior of the hydraulic system is effectively treated by the feedback linearization control [14]. To deal with parametric uncertainties, the adaptive mechanism is integrated into the nonlinear control design which adapts the unknown parameters based on the projection mapping function [12], [15]. To increase the robustness of the adaptive control under unmodeled disturbance and uncertain model parameters, the adaptive robust control (ARC) is proposed for a single-rod hydraulic actuator which guarantees bounded tracking performance [16]. Furthermore, the applications of ARC are realized in current works relating to not only valve-controlled hydraulic system, but also pump-controlled hydraulic system [17], and pump and valves combined hydraulic system [18]. However, under the assumption that the unmodeled disturbance and its derivative is bounded, asymptotic tracking performance can be

achieved by integrating a novel robust integral of the sign of the error (RISE) feedback in the adaptive backstepping control design [19]. To cancel or attenuate the effect of external disturbance on the system performance, disturbance, the DOB is proposed to estimate it with the assumption that its derivative is bounded [13], [20]–[22]. Compared to the adaptive mechanism, the disturbance estimation performance is completely guaranteed and does not depend on the tracking performance. However, in the above-mentioned works, the problems are limited in healthy working conditions, not faulty conditions, which not only severely influents the high-accuracy tracking performance, but also poses a threat to the system safety [23]–[26].

In the electrohydraulic system, there are many types of faults as actuator faults including internal leakage, external leakage, drop in supply pressure, and sensor faults including pressure sensor fault and position sensor fault [27], [28]. Among them, internal leakage fault is the most popular problem which has been widely considered in previous studies. In [29], a robust leakage detection algorithm has been proposed for the electrohydraulic actuators disturbed by model uncertainty and external disturbance by using an adaptive nonlinear observer and a decision-making mechanism. However, in this work, only a single actuator fault is considered with the fault detection problem. In [27], taking the advantage of the nonlinear unknown input observer (NUIO), model-based fault detection and isolation (FDI) scheme is proposed for a rudder servo system. Many types of faults are presented in this work including actuator faults and sensor faults with simulation and experimental validation. However, the simultaneous faulty conditions have not been investigated and the fault identification and FTC were not involved. In [30], an FTC design is proposed to effectively control a redundant hydraulic actuation system with internal leakage fault and force synchronization problem. However, in these studies, the problem of internal leakage fault is only considered for one-DOF system, which does not suffer from the nonlinear dynamics as the n-DOF mechanical system and limits the application of the proposed algorithm. To the best of authors' knowledge, the problem of internal leakage faults in n-DOF electrohydraulic servosystem has not been studied in previous works.

In a certain aspect, faults can be considered as parametric uncertainty or external disturbance that exceeds an allowable threshold [24], [31]. As a result, the approaches mentioned above to deal with modeling uncertainty and external disturbance can be utilized in the design of FTC [32]. Taking the advantages of these approaches, in recent years, some efforts are trying to integrate the DOB and adaptive mechanism into the control design to simultaneously handle external disturbance and unknown model parameters in a more effective way. In [33], Yao. et. al. proposed a backstepping control scheme using a combination of an extended state observer (ESO) and a parameter adaption with projection mapping for a double-rod hydraulic servo system where the adapted parameters are utilized in the design of the ESO. However, the approach seems not practical because the disturbance estimation error, which is unknown, is used in the design of the adaptive function to adapt the unknown model parameters. In contrast, in [34], Wang. et. al. proposed a nonlinear adaptive control with a novel ESO for estimating both matched and mismatched lumped disturbances and uncertainties for a hydraulic valve-controlled single-rod actuator system. Different from [33], the design of the proposed ESO only utilizes the nominal model parameters and the parameter adaption is adopted to update ''virtual'' nominal model parameters, which gives more freedom in the control design. However, there is no proof theory to guarantee the convergence of the adapted parameters to the physical ones. Overall, merging the DOB and parameter adaption law is still an open problem [14].

In this paper, the problem of internal leakage faults in an n-DOF electrohydraulic servo system is studied for the first time by a novel active fault tolerant control design system. In the normal control mode, the internal leakage fault detection is achieved based on a decision-making mechanism that compared the estimated matched disturbance from the ESO to a preset value. After the fault is detected, the controller is reconfigured, i.e., the ESO which is utilized to estimate the matched disturbance is turned off, and the online identification algorithm based on adaptive law is turned on to effectively estimate the internal leakage fault coefficient which is the dominant component compared to the matched disturbance due to the severity of its effects on the system performance. Based on this approach, merging the DOB and adaptive mechanism is achieved in this work to effectively take advantage of both techniques. Moreover, the proposed control scheme can handle not only single-fault conditions but also simultaneous-fault conditions and entirely decouple the faulty effect from a faulty actuator to the remaining actuators. To attenuate the effect of mismatched disturbances/uncertainties on the control system, another ESO is designed and integrated with the above-mentioned techniques in the backstepping framework. Based on the Lyapunov stability analysis, bounded tracking performance is guaranteed. To verify the effectiveness of the proposed FTC, numerical simulations are conducted using a 2-DOF hydraulic manipulator model. The simulation results show that the proposed approach achieves acceptable tracking performance under a bunch of faulty conditions and difficulties.

This paper is organized as follows. In Section II, a general mathematical model of the n-DOF hydraulic system is presented. The fault detection and FTC design are developed in Section III. Stability analysis is conducted in Section IV and numerical simulation is presented in Section V. Finally, section VI concludes this paper.

II. SYSTEM MODELLING

A. MECHANICAL SYSTEM

The general structure of an n-DOF series-type manipulator is described in FIGURE 1. The dynamics of the n-DOF

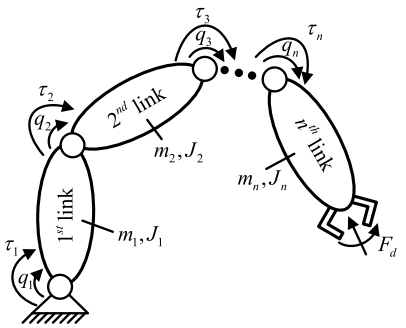

FIGURE 1. Schematic diagram of an n-DOF manipulator.

manipulator is given by [35], [36]

$$\boldsymbol{M}(\boldsymbol{q})\ddot{\boldsymbol{q}} + \boldsymbol{C}(\boldsymbol{q}, \dot{\boldsymbol{q}})\dot{\boldsymbol{q}} + \boldsymbol{G}(\boldsymbol{q}) + \boldsymbol{\tau}_d = \boldsymbol{\tau} \tag{1}$$

where $\boldsymbol{q}$ is the joint displacement vector, $\boldsymbol{M}(\boldsymbol{q}) \in \boldsymbol{R}^{n\times n}$ is the nominal inertia matrix which is symmetric positive-define, $\boldsymbol{C}(\boldsymbol{q}, \dot{\boldsymbol{q}})\dot{\boldsymbol{q}} \in \boldsymbol{R}^n$ represents the nominal vector of centrifugal and Coriolis moments, $\boldsymbol{G}(\boldsymbol{q}) \in \boldsymbol{R}^n$ is the nominal vector of gravity, $\boldsymbol{\tau}_d \in \boldsymbol{R}^n$ denotes the lumped disturbance and uncertainty in the mechanical system, and $\boldsymbol{\tau} \in \boldsymbol{R}^n$ is the actuator force/torque vector.

Assumption 1: The Coulomb friction is assumed to be differentiable, which is proportional to the function tanh(•), instead of the signum function sgn(•), where (•) is the investigated velocity [36], [37].

Based on Assumption 1, the vector $\boldsymbol{\tau}_d$ including parametric uncertainty, viscous friction, Coulomb friction, and external disturbance $\boldsymbol{F}_d$ is expressed as below

$$\begin{aligned}\boldsymbol{\tau}_d = {} & \Delta\boldsymbol{M}(\boldsymbol{q})\ddot{\boldsymbol{q}} + \Delta\boldsymbol{C}(\boldsymbol{q}, \dot{\boldsymbol{q}})\dot{\boldsymbol{q}} + \Delta\boldsymbol{G}(\boldsymbol{q}) \\ & + \boldsymbol{B}_v\dot{\boldsymbol{q}} + \boldsymbol{B}_C \tanh(\dot{\boldsymbol{q}}) - \boldsymbol{J}^T\boldsymbol{F}_d\end{aligned} \tag{2}$$

where $\Delta\boldsymbol{M}$, $\Delta\boldsymbol{C}$, and $\Delta\boldsymbol{G}$ denotes uncertain matrices and vectors caused by model parameter uncertainties. $\boldsymbol{B}_v$ and $\boldsymbol{B}_C$ represent the unknown viscous and Coulomb friction matrices of the joints. The Jacobian matrix $\boldsymbol{J} = \partial\boldsymbol{x}_E/\partial\boldsymbol{q}$ is defined based on the relation between end-effector position $\boldsymbol{x}_E$ and joint angles $\boldsymbol{q}$.

The actuator force/torque $\boldsymbol{\tau}$ is computed based on the force/torque generated by the hydraulic power as

$$\begin{aligned}\boldsymbol{\tau} &= \boldsymbol{J}_a^T(\boldsymbol{q})(\boldsymbol{F} - \boldsymbol{F}_a) \\ \boldsymbol{F}_a &= \boldsymbol{D}_v\boldsymbol{J}_a(\boldsymbol{q})\dot{\boldsymbol{q}} + \boldsymbol{D}_C \tanh(\boldsymbol{J}_a(\boldsymbol{q})\dot{\boldsymbol{q}})\end{aligned} \tag{3}$$

where $\boldsymbol{D}_v, \boldsymbol{D}_C$ denote the viscous friction and Coulomb friction matrices of the actuator. The Jacobian matrix from manipulator space to actuator space $\boldsymbol{J}_a = \partial\boldsymbol{c}/\partial\boldsymbol{q}$ is calculated based on the geometric relation between joint angles $\boldsymbol{q}$ and actuator displacements $\boldsymbol{c}$.

From (1)-(3), the manipulator dynamics is re-written as

$$\boldsymbol{M}(\boldsymbol{q})\ddot{\boldsymbol{q}} + \boldsymbol{C}(\boldsymbol{q}, \dot{\boldsymbol{q}})\dot{\boldsymbol{q}} + \boldsymbol{G}(\boldsymbol{q}) + \boldsymbol{d} = \boldsymbol{J}_a^T(\boldsymbol{q})\boldsymbol{F} \tag{4}$$

where $\boldsymbol{d} = \boldsymbol{\tau}_d + \boldsymbol{J}_a^T(\boldsymbol{q})\boldsymbol{F}_a$ represents lumped disturbance and uncertainty vector.

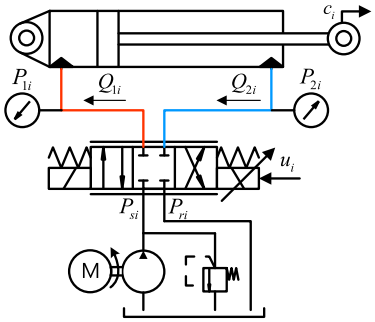

FIGURE 2. A typical electrohydraulic actuation system.

B. HYDRAULIC SYSTEM

A typical electrohydraulic actuation system is described in FIGURE 2 including a 4-way-3-position servo valve and a hydraulic actuator which can be a cylinder or a rotary actuator. The force/torque generated by the i^{th} hydraulic actuator as mentioned in (3) and (4) is computed by

$$F_i = A_{1i}P_{1i} - A_{2i}P_{2i} \tag{5}$$

where P_{1i} and P_{2i} are the pressures of both chambers. A_{1i} and A_{2i} denote the areas of both sides of the actuator.

The pressure dynamics of each actuator is given as [13]

$$\begin{aligned}\dot{P}_{1i} &= \frac{\beta_e}{V_{1i}}\left(-A_{1i}J_{ai}\dot{q}_i - q_{Li} + Q_{1i}\right) + w_{1i} \\ \dot{P}_{2i} &= \frac{\beta_e}{V_{2i}}\left(A_{2i}J_{ai}\dot{q}_i + q_{Li} - Q_{2i}\right) + w_{2i}\end{aligned} \tag{6}$$

where $V_{1i} = V_{01i} + A_{1i}c_i$ and $V_{2i} = V_{02i} - A_{2i}c_i$ are the volumes trapped in both chambers of the i^{th} cylinder ($i = \overline{1,n}$) while V_{01i} and V_{02i} are the initial volumes. β_e denotes the nominal value of Bulk modulus. q_{Li}, Q_{1i}, Q_{2i}, and w_{1i}, w_{2i} denote the internal leakage flow rate, flow rates going to/from both chambers, and the modeling errors in the pressure dynamics of the i^{th} actuator, respectively.

The internal leakage is modeled as follows:

$$q_{Li} = C_{0i}(P_{1i} - P_{2i}) + C_{ti}\sqrt{P_{1i} - P_{2i}}\,\text{sgn}(P_{1i} - P_{2i}) \tag{7}$$

where C_{0i} is a known coefficient and C_{ti} is an unknown faulty coefficient. When C_{ti} is large enough, the internal leakage fault happens and seriously affects the system performance.

With the assumption that the spool dynamics is neglected, i.e., $x_{vi} = k_{ui}u_i$ where u_i is the control signal which is the voltage applied to the i^{th} servo valve, the supplied flow rate to the 1st chamber and the return flow rate of the 2nd chamber are derived by

$$\begin{aligned}Q_{1i} &= k_{qi}k_{ui}u_i[s^*(u_i)\sqrt{P_{si} - P_{1i}} + s^*(-u_i)\sqrt{P_{1i} - P_{ri}}] \\ Q_{2i} &= k_{qi}k_{ui}u_i[s^*(u_i)\sqrt{P_{2i} - P_{ri}} + s^*(-u_i)\sqrt{P_{si} - P_{2i}}]\end{aligned} \tag{8}$$

where k_{qi} is the hydraulic coefficient depending on the discharge coefficient, spool valve area gradient, and the density of the oil. The function $s^*(x)$ is defined as

$$s^*(x) = \begin{cases}1, & \text{if } x \geq 0 \\ 0, & \text{if } x < 0\end{cases} \tag{9}$$

C. TOTAL SYSTEM

To consider both the mechanical system and hydraulic system, a new state variable is defined as $\boldsymbol{x} = [\boldsymbol{q}^T, \dot{\boldsymbol{q}}^T, (\boldsymbol{A}_1\boldsymbol{P}_1 - \boldsymbol{A}_2\boldsymbol{P}_2)^T]^T$. The total system model can be summarized as follows:

$$\begin{cases} \dot{\boldsymbol{x}}_1 = \boldsymbol{x}_2 \\ \dot{\boldsymbol{x}}_2 = \boldsymbol{M}(\boldsymbol{x}_1)^{-1}(\boldsymbol{J}_a(\boldsymbol{x}_1)^T\boldsymbol{x}_3 - \boldsymbol{C}(\boldsymbol{x}_1,\boldsymbol{x}_2)\boldsymbol{x}_2 - \boldsymbol{G}(\boldsymbol{x}_1) - \boldsymbol{d}) \\ \dot{\boldsymbol{x}}_3 = \boldsymbol{f}_1(\boldsymbol{x}_1)\boldsymbol{u} - \boldsymbol{f}_2(\boldsymbol{x}_1,\boldsymbol{x}_2) - \boldsymbol{f}_3(\boldsymbol{x}_1)\boldsymbol{C}_t + \boldsymbol{f} \end{cases} \tag{10}$$

where $\boldsymbol{A}_1 = \text{diag}\,(A_{11}, A_{12}, \ldots A_{1n})$; $\boldsymbol{A}_2 = \text{diag}\,(A_{21}, A_{22}, \ldots A_{2n})$; $\boldsymbol{C}_t = [C_{t1}, C_{t2}, \ldots, C_{tn}]^T$; $\boldsymbol{P}_1 = [P_{11}, P_{12}, \ldots, P_{1n}]^T$; $\boldsymbol{P}_2 = [P_{21}, P_{22}, \ldots\ldots, P_{2n}]^T$; $\boldsymbol{f}_1 = \text{diag}(f_{11}, f_{12}, \ldots, f_{1n})$; $\boldsymbol{f}_2 = [f_{21}, f_{22}, \ldots, f_{2n}]^T$; $\boldsymbol{f}_3 = \text{diag}(f_{31}, f_{32}, \ldots, f_{3n})$; $\boldsymbol{f} = \text{diag}(f_1, f_2, \ldots, f_n)$.

The detailed description of each element in the above matrices and vectors is given as

$$\begin{aligned} f_{1i} &= \frac{A_{1i}\beta_e}{V_{1i}} k_{qi}k_{ui}R_{1i} + \frac{A_{2i}\beta_e}{V_{2i}} k_{qi}k_{ui}R_{2i} \\ f_{2i} &= \frac{A_{1i}\beta_e}{V_{1i}} \left[A_{1i}J_{aii}x_{2i} + C_{0i}\left(P_{1i} - P_{2i}\right)\right] \\ &\quad + \frac{A_{2i}\beta_e}{V_{2i}} \left[A_{2i}J_{aii}x_{2i} + C_{0i}\left(P_{1i} - P_{2i}\right)\right] \\ f_{3i} &= \left(\frac{A_{1i}\beta_e}{V_{1i}} + \frac{A_{2i}\beta_e}{V_{2i}}\right) \sqrt{|P_{1i} - P_{2i}|}\,\text{sgn}\left(P_{1i} - P_{2i}\right) \\ f_i &= A_{1i}w_{1i} - A_{2i}w_{2i} \\ R_{1i} &= s^*\left(u_i\right)\sqrt{P_{si} - P_{1i}} + s^*\left(-u_i\right)\sqrt{P_{1i} - P_{ri}} \\ R_{2i} &= s^*\left(u_i\right)\sqrt{P_{2i} - P_{ri}} + s^*\left(-u_i\right)\sqrt{P_{si} - P_{2i}} \end{aligned} \tag{11}$$

Assumption 2: $\boldsymbol{x}_1, \boldsymbol{P}_1, \boldsymbol{P}_2$ are the outputs of the system which are measured by sensors. All system states, their 1st derivatives, and all elements in the matrices $\boldsymbol{M}(\boldsymbol{x_1})$ and $\boldsymbol{J_a}(\boldsymbol{x_1})$ are bounded.

Assumption 3: The following Lipschitz conditions hold

$$\begin{aligned} |f_{2i}(x_{1i}, x_{2i} + \Delta x_{2i}) - f_{2i}(x_{1i}, x_{2i})| &\le \kappa_i\,|\Delta x_{2i}| \\ \|\boldsymbol{C}(\boldsymbol{x}_1, \boldsymbol{x}_2 + \Delta x_2)(\boldsymbol{x}_2 + \Delta x_2) - \boldsymbol{C}(\boldsymbol{x}_1, \boldsymbol{x}_2)\boldsymbol{x}_2\| &\le \kappa\,\|\Delta x_2\| \end{aligned} \tag{12}$$

where κ_i and κ are positive constants.

Assumption 4: The lumped disturbance/uncertainty term $\boldsymbol{f}$ is bounded, i.e., $|f_i| \le \Delta_i^f$ where Δ_i^f is a constant.

Remark 1: Based on assumption 1, the derivative of $\boldsymbol{x}_1$, i.e., $\boldsymbol{x}_2$, and the derivative of the load pressure $\dot{\boldsymbol{x}}_3$ are calculated based on the well-known Levant's exact differentiator with a very small bounded calculation error [38]. The differential quantity $(\bullet)$ computed by Levant's differentiator is denoted by $\overline{(\bullet)}$. For the sake of condense, the derivation of it is omitted in this work.

III. FAULT DETECTION AND FAULT TOLERANT CONTROL DESIGN

The proposed FTC scheme is described in FIGURE 3 including the mismatched DOB, matched DOB, online identification, fault detection, and control reconfiguration mechanism. A full state feedback backstepping control is the main controller to guarantee the position tracking performance of the n-DOF hydraulic system under both healthy conditions and faulty conditions.

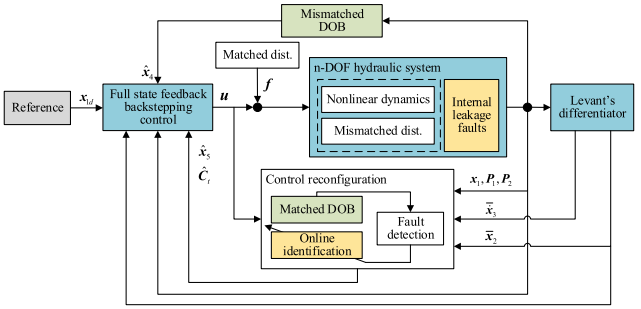

FIGURE 3. Proposed active FTC scheme.

Lemma 1: Consider a time-varying positive quantity $X(t)$. One concludes that $X(t)$ will stay in a bounded region that $X(t) \le b/a$ when $t \to \infty$ if there exist positive constants a and b that satisfies

$$\dot{X} \le -aX + b \tag{13}$$

Proof: Multiplying both sides of (13) by e^{at} and taking the integral of them, one obtains

$$X(t) \le \left(X(0) - \frac{b}{a}\right)e^{-at} + \frac{b}{a} \tag{14}$$

Because $\lim_{t\to\infty} e^{-at} = 0$, Lemma 1 is proved.

A. DISTURBANCE OBSERVER DESIGN

To design the matched DOB and mismatched DOB, the extended-state mechanism is adopted to generate 2 augmented state-space equations as follows:

$$\begin{cases} \dot{\boldsymbol{x}}_1 = \boldsymbol{x}_2 \\ \dot{\boldsymbol{x}}_2 = \boldsymbol{M}(\boldsymbol{x}_1)^{-1}(\boldsymbol{J}_a(\boldsymbol{x}_1)^T\boldsymbol{x}_3 \\ \qquad -\boldsymbol{C}(\boldsymbol{x}_1,\boldsymbol{x}_2)\boldsymbol{x}_2 - \boldsymbol{G}(\boldsymbol{x}_1)) + \boldsymbol{x}_4 \\ \dot{\boldsymbol{x}}_4 = \boldsymbol{h}_1 \end{cases} \tag{15}$$

$$\begin{cases} \dot{\boldsymbol{x}}_3 = \boldsymbol{f}_1(\boldsymbol{x}_1)\boldsymbol{u} - \boldsymbol{f}_2(\boldsymbol{x}_1,\boldsymbol{x}_2) + \boldsymbol{x}_5 \\ \dot{\boldsymbol{x}}_5 = \boldsymbol{h}_2 \end{cases} \tag{16}$$

where $\boldsymbol{x}_4 = -\boldsymbol{M}(\boldsymbol{x}_1)^{-1}\boldsymbol{d}$; $\boldsymbol{x}_5 = \boldsymbol{f} - \boldsymbol{f}_3\boldsymbol{C}_t$.

Assumption 5: The derivatives of lumped disturbances are bounded, i.e., $\|\boldsymbol{h}_1\| \le \delta_1$, $\|\boldsymbol{h}_2\| \le \delta_2$ where δ_1 and δ_2 are positive constants.

To simplify the design of mismatched disturbance observer for the system (15), the state equation is re-written as

$$\begin{cases} \dot{\boldsymbol{x}}_{e1} = \boldsymbol{A}_{e1}\boldsymbol{x}_{e1} + \boldsymbol{F}_{e1}\left(\boldsymbol{x}_1, \boldsymbol{x}_2, \boldsymbol{x}_3\right) + \boldsymbol{\Psi}_{e1} \\ \boldsymbol{y}_{e1} = \boldsymbol{C}_{e1}\boldsymbol{x}_{e1} \end{cases} \tag{17}$$

where

$$\begin{aligned} \boldsymbol{A}_{e1} &= \begin{bmatrix} 0_{n\times n} & \boldsymbol{I}_n & 0_{n\times n} \\ 0_{n\times n} & 0_{n\times n} & \boldsymbol{I}_n \\ 0_{n\times n} & 0_{n\times n} & 0_{n\times n} \end{bmatrix}; \boldsymbol{\Psi}_{e1} = \begin{bmatrix} 0_{n\times 1} \\ 0_{n\times 1} \\ \boldsymbol{h}_1 \end{bmatrix} \\ \boldsymbol{F}_{e1} &= \begin{bmatrix} 0_{n\times 1} \\ \boldsymbol{M}(\boldsymbol{x}_1)^{-1}(\boldsymbol{J}_a(\boldsymbol{x}_1)^T\boldsymbol{x}_3 \\ \qquad -\boldsymbol{C}(\boldsymbol{x}_1,\boldsymbol{x}_2)\boldsymbol{x}_2 - \boldsymbol{G}(\boldsymbol{x}_1)) \\ 0_{n\times 1} \end{bmatrix}; \\ \boldsymbol{C}_{e1} &= \begin{bmatrix} \boldsymbol{I}_n & 0_{n\times n} & 0_{n\times n} \end{bmatrix}; \boldsymbol{x}_{e1} = [\boldsymbol{x}_1^T, \boldsymbol{x}_2^T, \boldsymbol{x}_4^T]^T \end{aligned} \tag{18}$$

The mismatched disturbance observer is designed as follows:

$$\begin{aligned}\dot{\hat{\boldsymbol{x}}}_{e1} &= \boldsymbol{A}_{e1}\hat{\boldsymbol{x}}_{e1} + \boldsymbol{F}_{e1}\left(\boldsymbol{x}_1, \bar{\boldsymbol{x}}_2, \boldsymbol{x}_3\right) + \boldsymbol{L}_{e1}\left(\boldsymbol{y}_{e1} - \hat{\boldsymbol{y}}_{e1}\right)\\ \hat{\boldsymbol{y}}_{e1} &= \boldsymbol{C}_{e1}\hat{\boldsymbol{x}}_{e1}\end{aligned} \tag{19}$$

where $\boldsymbol{L}_{e1} = [3\omega_{e1}\boldsymbol{I}_n, 3\omega_{e1}^2\boldsymbol{I}_n, \omega_{e1}^3\boldsymbol{I}_n]^T$ is the observer gain, ω_{e1} is the bandwidth of the disturbance observer.

Theorem 1: For the system (17), the disturbance observer (19) guarantees a small bounded estimation performance of the mismatched disturbance $\boldsymbol{x}_4$ if the bandwidth of the observer ω_{e1} is chosen with a large enough value.

Proof of Theorem 1: See Appendix.

Similarly, to design a matched disturbance observer for the system (16), the state equation is re-written as

$$\begin{cases}\dot{\boldsymbol{x}}_{e2} = \boldsymbol{A}_{e2}\boldsymbol{x}_{e2} + \boldsymbol{F}_{e2}(\boldsymbol{x}_1, \boldsymbol{x}_2) + \boldsymbol{B}_{e2}(\boldsymbol{x}_1)\boldsymbol{u} + \boldsymbol{\Psi}_{e2}\\ \boldsymbol{y}_{e2} = \boldsymbol{C}_{e2}\boldsymbol{x}_{e2}\end{cases} \tag{20}$$

where

$$\boldsymbol{A}_{e2} = \begin{bmatrix}0_{n\times n} & \boldsymbol{I}_n\\ 0_{n\times n} & 0_{n\times n}\end{bmatrix};\ \boldsymbol{F}_{e2} = \begin{bmatrix}-\boldsymbol{f}_2\left(\boldsymbol{x}_1, \boldsymbol{x}_2\right)\\ 0_{n\times 1}\end{bmatrix};$$
$$\boldsymbol{B}_{e2} = \begin{bmatrix}\boldsymbol{f}_1\left(\boldsymbol{x}_1\right)\\ 0_{n\times n}\end{bmatrix}$$
$$\boldsymbol{\Psi}_{e2} = \begin{bmatrix}0_{n\times 1}\\ \boldsymbol{h}_2\end{bmatrix};\ \boldsymbol{C}_{e2} = \begin{bmatrix}\boldsymbol{I}_n\ 0_{n\times n}\end{bmatrix};\ \boldsymbol{x}_{e1} = [\boldsymbol{x}_3^T, \boldsymbol{x}_5^T]^T$$

A matched disturbance observer is designed by

$$\begin{aligned}\dot{\hat{\boldsymbol{x}}}_{e2} &= \boldsymbol{A}_{e2}\hat{\boldsymbol{x}}_{e2} + \boldsymbol{F}_{e2}(\boldsymbol{x}_1, \bar{\boldsymbol{x}}_2) + \boldsymbol{B}_{e2}(\boldsymbol{x}_1)\boldsymbol{u} + \boldsymbol{L}_{e2}\left(\boldsymbol{y}_{e2} - \hat{\boldsymbol{y}}_{e2}\right)\\ \hat{\boldsymbol{y}}_{e2} &= \boldsymbol{C}_{e2}\hat{\boldsymbol{x}}_{e2}\end{aligned} \tag{21}$$

where $\boldsymbol{L}_{e2} = [2\omega_{e2}\boldsymbol{I}_n, \omega_{e2}^2\boldsymbol{I}_n]^T$ is the observer gain, ω_{e2} is the observer bandwidth.

Theorem 2: For the system (20), the disturbance observer (21) guarantees a small bounded estimation performance of the matched disturbance $\boldsymbol{x}_5$ if the observer bandwidth ω_{e2} is chosen with a large enough value.

Proof of Theorem 2: Similar to Proof of Theorem 1. See Appendix.

B. ONLINE-FAULT IDENTIFICATION

In this section, the online-fault identification algorithm is proposed based on the adaptive mechanism with the linear regression [39]. However, instead of estimating both the internal leakage fault coefficients and the remaining unstructured uncertainty term, only the internal leakage fault coefficients are considered to simplify the algorithm but still achieve the identification performance.

Considering the 3rd equation of the system dynamics (10), one obtains the corresponding model as follows:

$$\boldsymbol{z} = \boldsymbol{f}_1(\boldsymbol{x}_1)\boldsymbol{u} - \boldsymbol{f}_2(\boldsymbol{x}_1, \boldsymbol{x}_2) - \boldsymbol{f}_3(\boldsymbol{x}_1)\boldsymbol{C}_t + \boldsymbol{f} \tag{22}$$

where $\boldsymbol{z} = \dot{\bar{\boldsymbol{x}}}_3$.

The prediction model is designed by

$$\hat{\boldsymbol{z}} = \boldsymbol{f}_1(\boldsymbol{x}_1)\boldsymbol{u} - \boldsymbol{f}_2(\boldsymbol{x}_1, \bar{\boldsymbol{x}}_2) - \boldsymbol{f}_3(\boldsymbol{x}_1)\hat{\boldsymbol{C}}_t \tag{23}$$

Denote the prediction error $\tilde{\boldsymbol{z}} = \boldsymbol{z} - \hat{\boldsymbol{z}}$. The online identification for internal leakage fault based on adaptive law is proposed as

$$\dot{\hat{\boldsymbol{C}}}_t = -\boldsymbol{\Gamma}\boldsymbol{f}_3^T\tilde{\boldsymbol{z}} \tag{24}$$

where $\boldsymbol{\Gamma}$ is a diagonal positive-definite matrix, which denotes the gain of the online identification algorithm.

Theorem 3: The bounded estimation performance $\tilde{\boldsymbol{C}}_t = \boldsymbol{C}_t - \hat{\boldsymbol{C}}_t$ can be obtained if the persistently exciting condition is satisfied, i.e.,

$$\forall t, \exists\alpha_0, \Delta t > 0: \int_t^{t+\Delta t} \boldsymbol{f}_3^T\boldsymbol{f}_3 dt \geq \alpha_0\boldsymbol{I}_n\Delta t \tag{25}$$

Proof of Theorem 3: See Appendix.

Remark 2: Different than most of the previous works using the adaptive mechanism to obtain the position tracking performance, the online identification law (24) guarantees bounded estimation performance and does not depend on the tracking error between system states and their desired values.

C. CONTROL DESIGN

A switching term $\boldsymbol{s} = \text{diag}(s_1, s_2, \ldots, s_n)$ is introduced here for fault detection based on the matched disturbance estimation values as follows:

$$s_i = \begin{cases}0, & \text{if } \left|\hat{x}_{5i}\right| < \rho_i\\ 1, & \text{if } \left|\hat{x}_{5i}\right| \geq \rho_i\end{cases} \tag{26}$$

where ρ_i is a pre-defined threshold.

Remark 3: The switching term (26) is not only used for fault detection but also used to activate the adaptive law (24) and deactivate the matched observer (21) when faults are detected. Furthermore, it is well integrated into the fault-tolerant control design in the following steps.

Step 1: Define the position tracking error $\boldsymbol{z}_1 = \boldsymbol{x}_1 - \boldsymbol{x}_d$ where $\boldsymbol{x}_d$ is a reference trajectory. Considering the first equation of (10), the derivative of $\boldsymbol{z}_1$ becomes

$$\dot{\boldsymbol{z}}_1 = \boldsymbol{x}_2 - \dot{\boldsymbol{x}}_d \tag{27}$$

To obtain asymptotically tracking performance of $\boldsymbol{z}_1$, a virtual control law of $\boldsymbol{x}_2$ is designed as follows:

$$\boldsymbol{\alpha}_1 = \dot{\boldsymbol{x}}_d - k_1\boldsymbol{z}_1 \tag{28}$$

where k_1 is a positive constant.

Step 2: Define the error between $\boldsymbol{x}_2$ and the virtual control law $\boldsymbol{\alpha}_1$ by $\boldsymbol{z}_2 = \boldsymbol{x}_2 - \boldsymbol{\alpha}_1$. From the second equation of (10), the derivative of $\boldsymbol{z}_2$ is expressed as

$$\begin{aligned}\dot{\boldsymbol{z}}_2 = \boldsymbol{M}(\boldsymbol{x}_1)^{-1}(\boldsymbol{J}_a(\boldsymbol{x}_1)^T\boldsymbol{x}_3 - \boldsymbol{C}(\boldsymbol{x}_1, \boldsymbol{x}_2)\boldsymbol{x}_2\\ -\boldsymbol{G}(\boldsymbol{x}_1) - \boldsymbol{d}) - \dot{\boldsymbol{\alpha}}_1\end{aligned} \tag{29}$$

From (29), the virtual control law of $\boldsymbol{x}_3$ is designed as

$$\begin{aligned}\boldsymbol{\alpha}_2 = \boldsymbol{J}_a(\boldsymbol{x}_1)^{-T}(\boldsymbol{C}(\boldsymbol{x}_1, \bar{\boldsymbol{x}}_2)\bar{\boldsymbol{x}}_2 + \boldsymbol{G}(\boldsymbol{x}_1)\\ +\boldsymbol{M}(\boldsymbol{x}_1)(\dot{\boldsymbol{\alpha}}_1 - \boldsymbol{z}_1 - k_2\boldsymbol{z}_2 - \hat{\boldsymbol{x}}_4))\end{aligned} \tag{30}$$

where k_2 is a positive constant.

Step 3: Denote $\boldsymbol{z}_3 = \boldsymbol{x}_3 - \boldsymbol{\alpha}_2$. From the third equation of the total system (10), the derivative of it is calculated by

$$\dot{\boldsymbol{z}}_3 = \boldsymbol{f}_1(\boldsymbol{x}_1)\boldsymbol{u} - \boldsymbol{f}_2(\boldsymbol{x}_1, \boldsymbol{x}_2) - \boldsymbol{f}_3(\boldsymbol{x}_1)\boldsymbol{C}_t + \boldsymbol{f} - \dot{\boldsymbol{\alpha}}_2 \tag{31}$$

Hence, the control signal is proposed by

$$\boldsymbol{u} = \frac{1}{\boldsymbol{f}_1}(\boldsymbol{f}_2(\boldsymbol{x}_1, \bar{\boldsymbol{x}}_2) - (\boldsymbol{I}_n - \boldsymbol{s})\hat{\boldsymbol{x}}_5 + \boldsymbol{s}\boldsymbol{f}_3(\boldsymbol{x}_1)\hat{\boldsymbol{C}}_t + \dot{\boldsymbol{\alpha}}_2 - \boldsymbol{J}_a(\boldsymbol{x}_1)\boldsymbol{M}(\boldsymbol{x}_1)^{-T}\boldsymbol{z}_2 - k_3\boldsymbol{z}_3) \quad (32)$$

where k_3 is a positive constant.

IV. STABILITY ANALYSIS

Theorem 4: For the system (10), by using the control signal (32) with mismatched disturbance observer (19), matched disturbance observer (21), adaptive law for fault identification (24), and the fault detection (26), arbitrary bounded tracking performance is guaranteed under lumped disturbance/uncertainty and internal leakage faults.

Proof of Theorem 4:

Consider the following Lyapunov function

$$V = \frac{1}{2}\boldsymbol{z}_1^T\boldsymbol{z}_1 + \frac{1}{2}\boldsymbol{z}_2^T\boldsymbol{z}_2 + \frac{1}{2}\boldsymbol{z}_3^T\boldsymbol{z}_3 \quad (33)$$

Taking the derivative of it, one obtains

$$\begin{aligned}\dot{V} = {} & \boldsymbol{z}_1^T(\boldsymbol{z}_2 + \boldsymbol{\alpha}_1 - \dot{\boldsymbol{x}}_d) + \boldsymbol{z}_2^T(\boldsymbol{M}(\boldsymbol{x}_1)^{-1}(\boldsymbol{J}_a(\boldsymbol{x}_1)^T(\boldsymbol{z}_3 + \boldsymbol{\alpha}_2) \\ & - \boldsymbol{C}(\boldsymbol{x}_1, \boldsymbol{x}_2)\boldsymbol{x}_2 - \boldsymbol{G}(\boldsymbol{x}_1)) + \boldsymbol{x}_4 - \dot{\boldsymbol{\alpha}}_1) \\ & + \boldsymbol{z}_3^T(\boldsymbol{f}_1\boldsymbol{u} - \boldsymbol{f}_2 + (\boldsymbol{I}_n - \boldsymbol{s})\boldsymbol{x}_5 - \boldsymbol{s}\boldsymbol{f}_3\boldsymbol{C}_t + \boldsymbol{s}\boldsymbol{f} - \dot{\boldsymbol{\alpha}}_2) \quad (34)\end{aligned}$$

Substituting control signals (28), (30), (32) into (34), the equation becomes

$$\begin{aligned}\dot{V} = {} & -k_1\boldsymbol{z}_1^T\boldsymbol{z}_1 - k_2\boldsymbol{z}_2^T\boldsymbol{z}_2 - k_3\boldsymbol{z}_3^T\boldsymbol{z}_3 + \boldsymbol{z}_2^T\tilde{\boldsymbol{x}}_4 \\ & + \boldsymbol{z}_2^T\boldsymbol{M}(\boldsymbol{x}_1)^{-1}\boldsymbol{J}_a(\boldsymbol{x}_1)^T(\boldsymbol{C}(\boldsymbol{x}_1, \bar{\boldsymbol{x}}_2)\bar{\boldsymbol{x}}_2 - \boldsymbol{C}(\boldsymbol{x}_1, \boldsymbol{x}_2)\boldsymbol{x}_2) \\ & - \boldsymbol{z}_3^T(\boldsymbol{I}_n - \boldsymbol{s})\tilde{\boldsymbol{x}}_5 + \boldsymbol{z}_3^T\boldsymbol{s}(\boldsymbol{f} + \boldsymbol{f}_3\tilde{\boldsymbol{C}}_t) \\ & - \boldsymbol{z}_3^T\left(\boldsymbol{f}_2(\boldsymbol{x}_1, \boldsymbol{x}_2) - \boldsymbol{f}_2(\boldsymbol{x}_1, \bar{\boldsymbol{x}}_2)\right) \quad (35)\end{aligned}$$

Applying Young's inequality, the following inequalities hold

$$\begin{aligned}\boldsymbol{z}_2^T\tilde{\boldsymbol{x}}_4 &\le \frac{1}{2}\boldsymbol{z}_2^T\boldsymbol{z}_2 + \frac{1}{2}\tilde{\boldsymbol{x}}_4^T\tilde{\boldsymbol{x}}_4 \\ -\boldsymbol{z}_2^T\boldsymbol{H}^T\widetilde{\boldsymbol{C}\boldsymbol{x}}_2 &\le \frac{1}{2}\boldsymbol{z}_2^T\boldsymbol{z}_2 + \frac{1}{2}\widetilde{\boldsymbol{C}\boldsymbol{x}}_2^T\boldsymbol{H}\boldsymbol{H}^T\widetilde{\boldsymbol{C}\boldsymbol{x}}_2 \\ -\boldsymbol{z}_3^T(\boldsymbol{I}_n - \boldsymbol{s})\tilde{\boldsymbol{x}}_5 &\le \frac{1}{2}\boldsymbol{z}_3^T\boldsymbol{z}_3 + \frac{1}{2}\tilde{\boldsymbol{x}}_5^T(\boldsymbol{I}_n - \boldsymbol{s})^T(\boldsymbol{I}_n - \boldsymbol{s})\tilde{\boldsymbol{x}}_5 \\ \boldsymbol{z}_3^T\boldsymbol{s}(\boldsymbol{f} + \boldsymbol{f}_3\tilde{\boldsymbol{C}}_t) &\le \frac{1}{2}\boldsymbol{z}_3^T\boldsymbol{z}_3 + \frac{1}{2}(\boldsymbol{f} + \boldsymbol{f}_3\tilde{\boldsymbol{C}}_t)^T\boldsymbol{s}^T\boldsymbol{s}(\boldsymbol{f} + \boldsymbol{f}_3\tilde{\boldsymbol{C}}_t) \\ -\boldsymbol{z}_3^T\tilde{\boldsymbol{f}}_2 &\le \frac{1}{2}\boldsymbol{z}_3^T\boldsymbol{z}_3 + \frac{1}{2}\tilde{\boldsymbol{f}}_2^T\tilde{\boldsymbol{f}}_2 \quad (36)\end{aligned}$$

where $\boldsymbol{H} = \boldsymbol{M}(\boldsymbol{x}_1)^{-1}\boldsymbol{J}_a(\boldsymbol{x}_1)^T, \tilde{\boldsymbol{f}}_2 = \boldsymbol{f}_2(\boldsymbol{x}_1, \boldsymbol{x}_2) - \boldsymbol{f}_2(\boldsymbol{x}_1, \bar{\boldsymbol{x}}_2), \widetilde{\boldsymbol{C}\boldsymbol{x}}_2 = \boldsymbol{C}(\boldsymbol{x}_1, \boldsymbol{x}_2)\boldsymbol{x}_2 - \boldsymbol{C}(\boldsymbol{x}_1, \bar{\boldsymbol{x}}_2)\bar{\boldsymbol{x}}_2$.

From Theorems 1, 2 and 3, Assumptions 3 and 4, and Remark 1, there exists a constant δ satisfying below inequality

$$\begin{aligned}& \frac{1}{2}\tilde{\boldsymbol{x}}_4^T\tilde{\boldsymbol{x}}_4 + \frac{1}{2}\tilde{\boldsymbol{x}}_5^T(\boldsymbol{I}_n - \boldsymbol{s})^T(\boldsymbol{I}_n - \boldsymbol{s})\tilde{\boldsymbol{x}}_5 \\ & \quad + \frac{1}{2}(\boldsymbol{f} + \boldsymbol{f}_3\tilde{\boldsymbol{C}}_t)^T\boldsymbol{s}^T\boldsymbol{s}(\boldsymbol{f} + \boldsymbol{f}_3\tilde{\boldsymbol{C}}_t) + \frac{1}{2}\tilde{\boldsymbol{f}}_2^T\tilde{\boldsymbol{f}}_2 \\ & \quad + \frac{1}{2}\widetilde{\boldsymbol{C}\boldsymbol{x}}_2^T\boldsymbol{H}\boldsymbol{H}^T\widetilde{\boldsymbol{C}\boldsymbol{x}}_2 \le \delta \quad (37)\end{aligned}$$

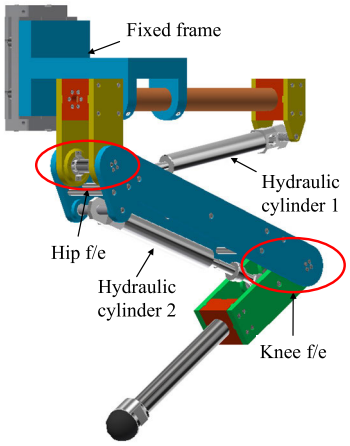

FIGURE 4. Diagram of the reduced HyQ leg prototype.

Substituting (36), (37) into (35), one obtains

$$\begin{aligned}\dot{V} &\le -k_1\boldsymbol{z}_1^T\boldsymbol{z}_1 - (k_2 - 1)\boldsymbol{z}_2^T\boldsymbol{z}_2 - \left(k_3 - \frac{3}{2}\right)\boldsymbol{z}_3^T\boldsymbol{z}_3 + \delta \\ &\le -\lambda V + \delta \quad (38)\end{aligned}$$

where $\lambda = \min(2k_1, 2k_2 - 2, 2k_3 - 3)$.

By using Lemma 1, with large enough control parameters k_1, k_2, and k_3 to make $\lambda > 0$, when $t \to \infty$, $V_3(t)$ will enter a region that $V_3(t) \le \delta/\lambda$ and Theorem 4 is proved.

Remark 4: Theoretically, the arbitrary bounded error can be achieved in both disturbance observer performance, adaptive fault identification performance, and tracking performance with large enough gains. However, the effect of sampling time is not considered here, which prevents the application of the high-gain observer, identifier, and controller in the real system. In other words, there is a trade-off between tracking/estimating performance and system stability.

V. NUMERICAL SIMULATION

In this section, the HyQ leg prototype developed by the University of Genoa, Italy, and the Italian Institute of Technology (IIT) is utilized to verify the effectiveness of the proposed FTC. The original model includes 2 hydraulic cylinders to actuate the hip flexion/extension (hip f/e) and the knee flexion/extension (knee f/e), and 1 electric motor to actuate the hip abduction/adduction (hip a/a). However, to be simple, the hip a/a joint is neglected here. The diagram of the reduced HyQ leg model is described in FIGURE 4. More details about testbench configuration can be found in [40], [41].

A. SIMULATION SETUP

To verify the performance of the proposed FTC, simulation results are conducted based on the 2-DOF hydraulic manipulator model as mentioned above. Parameters for the simulation are given in TABLE 1 and TABLE 2. Numerous model geometric parameters that are used to compute the kinematic problem are omitted here for simplicity, which can be found in [41].

TABLE 1. Mechanical parameters.

Symbol	Quantity	Value
m_1	Mass of link 1	1.77 kg
m_2	Mass of link 2	1.48 kg
J_{C1}	Inertia moment of link 1	0.0704 kgm^2
J_{C2}	Inertia moment of link 2	0.0486 kgm^2
l_1	Length of link 1	0.35 m
l_2	Length of link 2	0.35 m
b_{C1}	Coulomb friction of link 1	1 Nm
b_{C2}	Coulomb friction of link 2	1 Nm
b_{v1}	Viscous friction of link 1	10 Nm/(rad/s)
b_{v2}	Viscous friction of link 2	10 Nm/(rad/s)

The reference trajectory is chosen in a sinusoidal form as follows:

$$q_{1d} = -0.2 + 0.5\sin(4\pi t/3)\,(\text{rad})$$
$$q_{2d} = 1.4 + 0.5\sin(4\pi t/3)\,(\text{rad})$$

The mismatched disturbance includes unknown viscous and Coulomb friction at the revolute joints and the hydraulic cylinders as shown in TABLE 1 and TABLE 2, and the external load acting on the end effector is chosen as $\boldsymbol{F}_d = [10, -20]^T(1 - \exp(-t))$ (N).

The matched disturbance comes from unmodeled pressure dynamics, parameter deviations, and so on. Hence, in this simulation, the matched disturbance is considered as $f_i = 3.75 \times 10^7 \sin(2\pi t/3) + 1.25 \times 10^7 \sin(4\pi t/3)$ $(i = \overline{1,2})$.

To simulate the internal leakage faults in a practical system, the unknown leakage fault coefficients are selected as the following slow-varying components:

$$C_{t1} = \begin{cases} 0 & \text{if } t < 15\text{s} \\ 1.5 \times 10^{-9}(1 - e^{-0.5(t-15)}) & \text{if } t \geq 15\text{s} \end{cases}$$
$$C_{t2} = \begin{cases} 0 & \text{if } t < 25\text{s} \\ 0.7 \times 10^{-9}(1 - e^{-0.5(t-25)}) & \text{if } t \geq 25\text{s} \end{cases}$$

Remark 4: In practice, the control signals generated by the controller are limited due to the physical limitation of hardware components. Hence, they are bounded as below

$$u_{sat} = sat(u) = \begin{cases} u_{\max} & \text{if } u \geq u_{\max} \\ u_{\min} & \text{if } u \leq u_{\min} \\ u & \text{otherwise} \end{cases} \quad (39)$$

where $u_{\max} = 12\text{V}$,$u_{\min} = -12\text{V}$.

The structure of the simulation is described in FIGURE 5.

B. CONTROLLERS FOR COMPARISON

To evaluate the control performance of the proposed scheme for the hydraulic manipulator subjected to matched disturbance, mismatched disturbance, and severe internal leakage faults, the following three control algorithms are considered as follows:

TABLE 2. Hydraulic parameters.

Symbol	Quantity	Value
D	Bore diameter	0.016 m
d	Rod diameter	0.01 m
L	Stroke	0.08 m
A_1	Bore area	2.01 cm^2
A_2	Annulus area	1.23 cm^2
V_{01}	Initial volume of chamber 1	9.65 cm^3
V_{02}	Initial volume of chamber 2	5.88 cm^3
C_0	Nominal internal leakage coefficient	10^{-15}
k_u	Proportional gain of the valve	3×10^{-6} m/V
k_q	Hydraulic coefficient	4.65×10^{-4}
β_e	Bulk modulus	1.25 GPa
P_s	Supply pressure	160 bar
P_r	Return pressure	3 bar
d_{c1}	Coulomb friction of cylinder 1	5 N
d_{C2}	Coulomb friction of cylinder 2	5 N
d_{v1}	Viscous friction of cylinder 1	50 Ns/m
d_{v2}	Viscous friction of cylinder 2	50 Ns/m

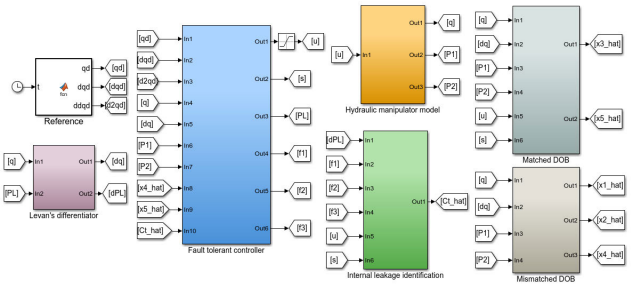

FIGURE 5. Structure of the simulation in MATLAB simulink.

1) Proposed control algorithm: The parameters of the proposed control algorithm are chosen as:

$$k_1 = 70, k_2 = 70, k_3 = 70,$$
$$\omega_{e1} = 150, \omega_{e2} = 100, \boldsymbol{\Gamma} = \text{diag}(10^{-28}, 10^{-28})$$

2) Backstepping control with 2 disturbance observers (BC2): This type of approach has been widely applied in previous works for the position tracking control of the hydraulic system [30], [33], [35]. In this controller, the control parameters are similar to those of the proposed controller but the online identification for internal leakage fault is neglected.
3) Backstepping control with mismatched disturbance observer and online identification based on the adaptive mechanism for internal leakage faults (BCA): This control method is inspired by previous work [39]. The control parameters are similar to those of the proposed controller but the matched DOB is neglected.

To effectively evaluate the control performance of the above-mentioned controllers, besides the well-known root-mean-square error (RMSE), the maximum, average, and

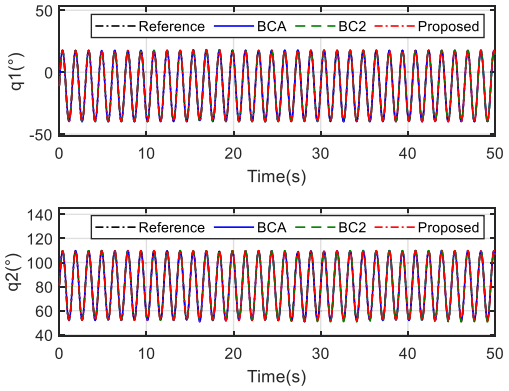

FIGURE 6. Position tracking performances of comparative controllers.

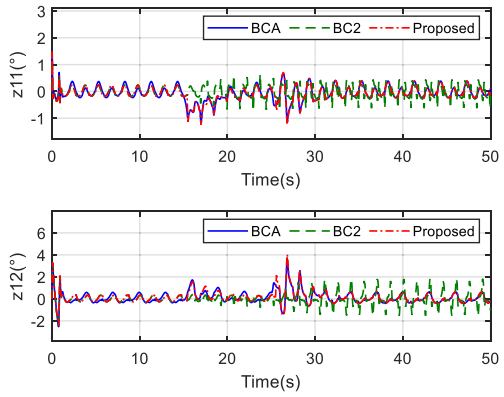

FIGURE 7. Position tracking errors of comparative controllers.

standard deviation of the tracking errors which are denoted as M_z, μ, and σ are utilized in this work [33].

C. SIMULATION RESULTS

The tracking performances of the proposed controller, BC2, and BSA are given in FIGURE 6. Both controllers guarantee that the angular displacement at each joint follows its reference trajectory. However, in FIGURE 7, the tracking error of each joint is clearly described which indicates that the proposed controller effectively takes advantage of both BC2 and BCA. During the period from 0s to 15s, i.e., before the faults occur, the tracking errors in both joints of the proposed controller and the BC2 are better than those of the BCA since the matched disturbance/uncertainty is the main problem. When the internal leakage faults occur at joint 1 and joint 2, the proposed controller switches from the BC2 to the BCA step-by-step. During this period, except for the transient response, the tracking performance of the proposed controller and the BCA is more accurate than it of the BC2 because the effects of the faulty conditions dominate the matched lumped disturbance effects in healthy conditions.

To quantitatively access the control performance of the comparative controllers in the steady-state phase, a similar simulation is conducted in 100s. The internal leakage faults in the 1st actuator and the 2nd actuator occur at 40s and 60s, respectively. The investigated periods include 30s in the steady-state phase of the healthy condition, i.e., from 10s to 40s, and 30s in the steady-state phase of the simultaneous faulty condition, i.e., from 70s to 100s. For the sake of simplicity, the steady-state phases of single internal leakage fault conditions are omitted here. The maximum, average, and standard deviation of the tracking errors are described in TABLE 3, TABLE 4, and TABLE 5, respectively. From these tables, it is obvious that the proposed controller inherits the advantages of both the BC2 and BCA in healthy conditions and faulty conditions, respectively. Furthermore, the RMSEs of three controllers are presented in TABLE 6, which once again proves the effectiveness of the proposed controller compared to the remaining controllers.

TABLE 3. Maximum of the tracking errors.

Control strategies	Joint 1 (Deg)		Joint 2 (Deg)	
	Heathy	Faulty	Healthy	Faulty
Proposed control	0.2383	0.3877	0.3759	0.6513
BC2	0.2382	0.6270	0.3757	1.8136
BCA	0.3694	0.3876	0.5921	0.6515

TABLE 4. Average of the tracking errors.

Control strategies	Joint 1 (Deg)		Joint 2 (Deg)	
	Heathy	Faulty	Healthy	Faulty
Proposed control	0.1343	0.1555	0.1948	0.2517
BC2	0.1342	0.2263	0.1954	0.5358
BCA	0.1453	0.1555	0.2455	0.2516

TABLE 5. Standard deviation of the tracking errors.

Control strategies	Joint 1 (Deg)		Joint 2 (Deg)	
	Heathy	Faulty	Healthy	Faulty
Proposed control	0.0646	0.0945	0.1002	0.1752
BC2	0.0646	0.1191	0.1004	0.5014
BCA	0.0938	0.0945	0.1580	0.1752

TABLE 6. RMSE of the tracking errors.

Control strategies	Joint 1 (Deg)		Joint 2 (Deg)	
	Heathy	Faulty	Healthy	Faulty
Proposed control	0.1490	0.1820	0.2191	0.3066
BC2	0.1490	0.2557	0.2196	0.7338
BCA	0.1729	0.1820	0.2920	0.3066

The fault detection signals are shown in FIGURE 8 based on the proposed decision-making mechanism (26). Compared to the identification performance described in FIGURE 9, it is obvious that the fault detection law effectively detects the faults in a very short time. After that, the online adaptive identification algorithm (24) successfully identifies the magnitude and shape of the fault as shown in FIGURE 9. The identification errors between the estimated values and the true values are generated by the matched lumped disturbance/uncertainty components and the imperfection when the faults are assumed to be slow-varying.

When the proposed controller is applied, the estimation performance of the mismatched disturbance observer is shown in FIGURE 10. The mismatched lumped disturbance/uncertainty term caused by the external force, unknown viscous friction, and unknown Coulomb friction acting at both rotating joints and hydraulic actuators are effectively estimated by the mismatched DOB (19). An interesting point can be observed that the mismatched disturbance is not affected by the internal leakage faults and matched

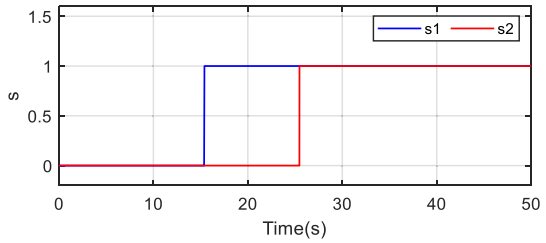

FIGURE 8. Fault detection performance.

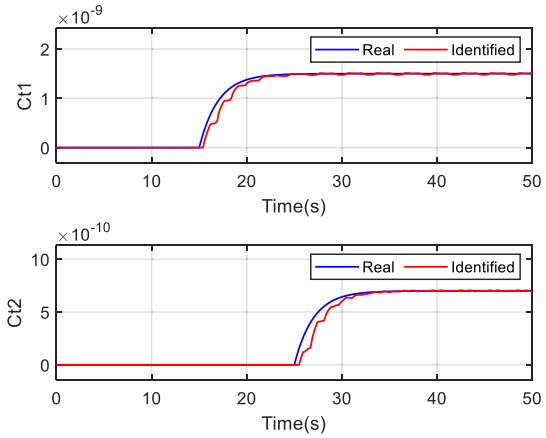

FIGURE 9. Internal leakage fault identification performance.

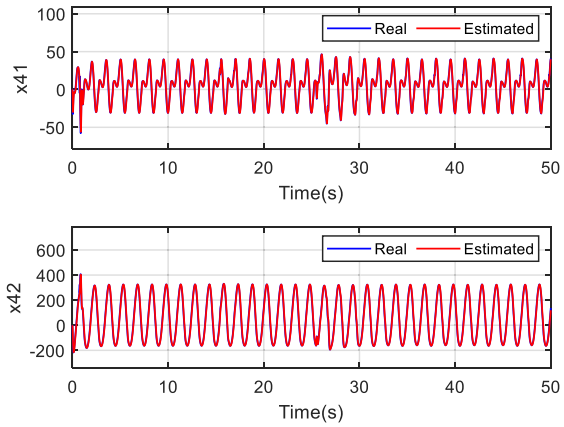

FIGURE 10. Mismatched lumped disturbance/uncertainty estimation performance.

disturbance in the hydraulic actuation system. It is reasonable because, in the design of the mismatched DOB (19), the load pressure is computed based on measured pressure signals, and supplied to the DOB, which isolates the problems in the hydraulic system from the mechanical system.

In FIGURE 11, when the proposed controller is applied, the matched disturbance terms in both joints are well estimated compared to the real term based on the matched DOB (21), even after the faults occur. At that time, although the lumped term is caused by both disturbance/uncertainty in healthy condition and internal leakage faults, the control performance of the BC2 is worse than it of the BCA and the proposed controller as mentioned before. Note that in the proposed controller, after the faults are detected, the matched DOB can be shut down. The estimation performance after that

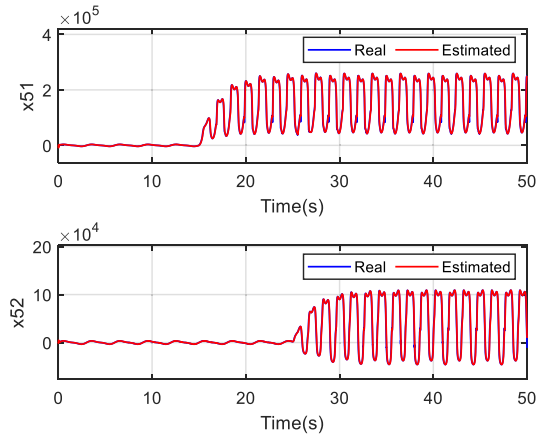

FIGURE 11. Matched lumped disturbance/uncertainty estimation performance.

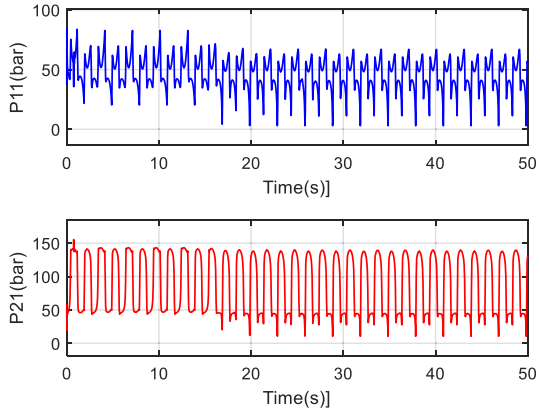

FIGURE 12. Pressures of both chambers in cylinder 1.

is shown in FIGURE 11 is only used to check the effectiveness of it under faulty conditions.

To evaluate the effect of faulty conditions on the hydraulic actuation system when the proposed control method is applied, the pressures of both chambers in actuator 1 and actuator 2 are shown in FIGURE 12 and FIGURE 13, respectively. In FIGURE 12, after the internal leakage fault occurs, the pressure of both chambers consequently changes. A similar situation is realized with the internal leakage fault in actuator 2, which is described in FIGURE 13. An interesting point that can be observed in these figures is that the faulty condition of an actuator does not affect the performance of the remaining actuator. This separation is achieved based on the compensation of mismatched DOB, matched DOB, the online adaptive identification, and the switching action of the fault detection law.

Finally, the control signals of both controllers are presented in FIGURE 14. One can observe that when the faults occur, the magnitude of the control signal increases. This situation is reasonable because when the internal leakage fault appears in an actuator, the leakage flow rate going from the high-pressure chamber to the low-pressure chamber severely rises, which reduces the load pressure and the actuator efficiency. Therefore, the control signals need to increase to compensate for the loss of effectiveness in actuators.

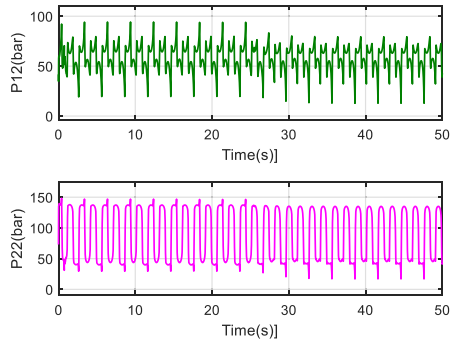

FIGURE 13. Pressure of both chambers in cylinder 2.

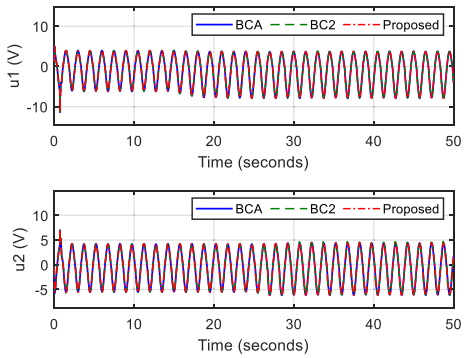

FIGURE 14. Control signals of comparative controllers.

VI. CONCONCLUSION

This paper proposes an active FTC system design for a hydraulic manipulator with internal leakage faults and matched/mismatched disturbances. A novel fault detection law is proposed to detect the internal leakage fault that occurs in each joint based on the estimated matched disturbances from the matched DOB. After that, an online adaptive identification algorithm is implemented to estimate the internal leakage fault coefficients. Besides, a mismatched DOB is designed to deal with the mismatched disturbance term caused by an external force, uncertain parameters, unknown viscous friction, and unknown Coulomb friction. The proposed FTC is designed based on the backstepping framework, which integrates the estimated values from DOBs and the identified fault information into the control system design. Thanks to the fault detection mechanism, the actuation performance of each joint is successfully decoupled from the total system, even under simultaneous faulty conditions. Moreover, the proposed controller takes the advantages of both DOBs, which are utilized to deal with disturbances, and the adaptive law, which is effective to handle the parametric uncertainty, in a unique framework. Simulation results show that compared to the BCA and BC2, the proposed controller presents the best tracking performance under both healthy conditions and simultaneous faulty conditions.

In future works, the following interesting problems shall be investigated in the active fault-tolerant control system design for hydraulic manipulator as

1) The transient response of the hydraulic manipulation system caused by the control reconfiguration action when the actuator fault occurs has not been considered in this work. Moreover, the transient response improvement has been studied in several works with different objects [42], [43], which motivates the study about similar problems in the hydraulic manipulators.
2) Other types of hydraulic actuator faults shall be researched in future works as the drop in pressure supply, valve proportional gain variation, etc. [27]. Moreover, depending on the structure of the hydraulic actuation system in the real applications including hydraulic actuators, hydraulic circuits, and hydraulic power source, not only the number of the actuator fault scenarios but also the effects of them on the entire system are very diverse but interesting to be investigated.
3) Besides the actuator faults, the sensor faults including position sensor faults and pressure sensor faults can pose a threat to the hydraulic manipulation control system. However, the effects of sensor faults on the hydraulic manipulator have not been considered in previous works. A few studies have focused on the sensor faults in hydraulic systems, but the degree of freedom is limited to one [44], [45]. Moreover, some studies have tried to solve the fault diagnosis problem in robot manipulators [46]–[48]. However, the actuator dynamics are neglected for simplicity.
4) Most of the current works focusing on the fault diagnosis and fault-tolerant control design for position tracking tasks. The effects of faulty conditions on the force control problems including direct force tracking control and indirect force control, i.e., impedance control, have not received much attention.

APPENDIX

PROOF OF THEOREM 1:

Define the estimation error $\tilde{\boldsymbol{x}}_{e1} = \boldsymbol{x}_{e1} - \hat{\boldsymbol{x}}_{e1}$. From (17), (18), the dynamics of estimation error is presented by

$$\dot{\tilde{\boldsymbol{x}}}_{e1} = (\boldsymbol{A}_{e1} - \boldsymbol{L}_{e1}\boldsymbol{C}_{e1})\tilde{\boldsymbol{x}}_{e1} + \boldsymbol{F}_{e1} - \bar{\boldsymbol{F}}_{e1} + \boldsymbol{\Psi}_{e1} \tag{40}$$

To be convenient, the scaled estimation error is defined as $\boldsymbol{\varepsilon}_{e1} = \tilde{\boldsymbol{x}}_1,\ \boldsymbol{\varepsilon}_{e2} = \tilde{\boldsymbol{x}}_2/\omega_{e1},\ \boldsymbol{\varepsilon}_{e3} = \tilde{\boldsymbol{x}}_4/\omega_{e1}^2$. Then, (40) can be rewritten as

$$\dot{\boldsymbol{\varepsilon}}_{e1} = \omega_{e1}\boldsymbol{A}_{\varepsilon 1}\boldsymbol{\varepsilon}_{e1} + \boldsymbol{B}_{\varepsilon 1}\frac{\widetilde{\boldsymbol{C}\boldsymbol{x}_2}}{\omega_{e1}} + \boldsymbol{B}_{\varepsilon 2}\frac{\boldsymbol{h}_1}{\omega_{e1}^2} \tag{41}$$

where $\boldsymbol{\varepsilon}_{e1} = [\boldsymbol{\varepsilon}_{e1}^T, \boldsymbol{\varepsilon}_{e2}^T, \boldsymbol{\varepsilon}_{e3}^T]^T$ and

$$\boldsymbol{A}_{\varepsilon 1} = \begin{bmatrix} -3\boldsymbol{I}_n & \boldsymbol{I}_n & 0_{n\times n} \\ -3\boldsymbol{I}_n & 0_{n\times n} & \boldsymbol{I}_n \\ -\boldsymbol{I}_n & 0_{n\times n} & 0_{n\times n} \end{bmatrix}; \boldsymbol{B}_{\varepsilon 1} = \begin{bmatrix} 0_{n\times n} \\ \boldsymbol{I}_n \\ 0_{n\times n} \end{bmatrix};$$

$$\boldsymbol{B}_{\varepsilon 2} = \begin{bmatrix} 0_{n\times n} \\ 0_{n\times n} \\ \boldsymbol{I}_n \end{bmatrix}$$

Since the matrix $\boldsymbol{A}_{\varepsilon 1}$ is Hurwitz, there exists a positive- definite matrix $\boldsymbol{P}_{\varepsilon 1}$ satisfying the Lyapunov equation as follows:

$$\boldsymbol{A}_{\varepsilon 1}^T\boldsymbol{P}_{\varepsilon 1} + \boldsymbol{P}_{\varepsilon 1}\boldsymbol{A}_{\varepsilon 1} = -2\boldsymbol{I}_{3n} \tag{42}$$

Consider the following Lyapunov function

$$V_{\varepsilon 1} = \frac{1}{2}\boldsymbol{\varepsilon}_{e1}^T \boldsymbol{P}_{\varepsilon 1}\boldsymbol{\varepsilon}_{e1} \tag{43}$$

Differentiating both sides of (43) and utilizing (42), the derivative of the Lyapunov function is given as

$$\dot{V}_{\varepsilon 1} = -\omega_{e1}\boldsymbol{\varepsilon}_{e1}^T\boldsymbol{\varepsilon}_{e1} + \boldsymbol{\varepsilon}_{e1}^T\boldsymbol{P}_{\varepsilon 1}\boldsymbol{B}_{\varepsilon 1}\frac{\widetilde{\boldsymbol{C}\boldsymbol{x}_2}}{\omega_{e1}} + \boldsymbol{\varepsilon}_{e1}^T\boldsymbol{P}_{\varepsilon 1}\boldsymbol{B}_{\varepsilon 2}\frac{\boldsymbol{h}_1}{\omega_{e1}^2} \tag{44}$$

Set $\boldsymbol{Y}_1 = \boldsymbol{B}_{\varepsilon 1}^T\boldsymbol{P}_{\varepsilon 1}^T\boldsymbol{P}_{\varepsilon 1}\boldsymbol{B}_{\varepsilon 1}$, $\boldsymbol{Y}_2 = \boldsymbol{B}_{\varepsilon 2}^T\boldsymbol{P}_{\varepsilon 1}^T\boldsymbol{P}_{\varepsilon 1}\boldsymbol{B}_{\varepsilon 2}$. From (44) and utilizing Young's inequality, the following inequality is derived as

$$\begin{aligned}\dot{V}_{\varepsilon 1} \le & -\omega_{e1}\boldsymbol{\varepsilon}_{e1}^T\boldsymbol{\varepsilon}_{e1} + \frac{1}{2}\boldsymbol{\varepsilon}_{e1}^T\boldsymbol{\varepsilon}_{e1} + \frac{1}{2\omega_{e1}^2}\widetilde{\boldsymbol{C}\boldsymbol{x}_2}^T\boldsymbol{Y}_1\widetilde{\boldsymbol{C}\boldsymbol{x}_2} \\ & + \frac{1}{2}\boldsymbol{\varepsilon}_{e1}^T\boldsymbol{\varepsilon}_{e1} + \frac{1}{2\omega_{e1}^4}\boldsymbol{h}_1^T\boldsymbol{Y}_2\boldsymbol{h}_1 \\ = & -(\omega_{e1}-1)\,\boldsymbol{\varepsilon}_{e1}^T\boldsymbol{\varepsilon}_{e1} + \frac{1}{2\omega_{e1}^2}\widetilde{\boldsymbol{C}\boldsymbol{x}_2}^T\boldsymbol{Y}_1\widetilde{\boldsymbol{C}\boldsymbol{x}_2} \\ & + \frac{1}{2\omega_{e1}^4}\boldsymbol{h}_1^T\boldsymbol{Y}_2\boldsymbol{h}_1 \end{aligned} \tag{45}$$

Combining (45) with Assumption 3 and Assumption 5, the following inequality holds

$$\dot{V}_{\varepsilon 1} \le -\lambda_{\varepsilon 1}V_{\varepsilon 1} + \frac{1}{2\omega_{e1}^4}\delta_{\varepsilon 1} \tag{46}$$

where

$$\begin{aligned}\lambda_{\varepsilon 1} &= 2\,(\omega_{e1}-1) \\ \delta_{\varepsilon 1} &= \sup(f_{\varepsilon 1}) \\ f_{\varepsilon 1} &= \omega_{e1}^2\lambda_{\max}(\boldsymbol{Y}_1)\widetilde{\boldsymbol{C}\boldsymbol{x}_2}^T\widetilde{\boldsymbol{C}\boldsymbol{x}_2} + \lambda_{\max}(\boldsymbol{Y}_2)\boldsymbol{h}_1^T\boldsymbol{h}_1 \end{aligned} \tag{47}$$

Note that when ω_{e1} increases, the term $f_{\varepsilon 1}$ also increases. However, based on Assumption 3 and the high accuracy of the Levant's differentiator as mentioned in Remark 1, this increase is very small and still bounded because ω_{e1} is limited as mentioned in Remark 4. Hence, the existence of the constant δ_{e1} is reasonable.

By using Lemma 1, when $t \to \infty$, $V_{\varepsilon 1}(t) \le \delta_{\varepsilon 1}/2\omega_{\varepsilon 1}^4\lambda_{\varepsilon 1}$, which leads to

$$\|\boldsymbol{\varepsilon}_{e1}\| \le \sqrt{\frac{\delta_{\varepsilon 1}}{\omega_{e1}^4\lambda_{\varepsilon 1}}} \tag{48}$$

From (47), (48) and the definition of the scaled estimation error, the following inequalities hold

$$\begin{aligned}\|\tilde{\boldsymbol{x}}_1\| &\le \frac{1}{\omega_{e1}^{5/2}}\sqrt{\frac{\delta_{\varepsilon 1}}{2\left(1-\frac{1}{\omega_{e1}}\right)}} \\ \|\tilde{\boldsymbol{x}}_2\| &\le \frac{1}{\omega_{e1}^{3/2}}\sqrt{\frac{\delta_{\varepsilon 1}}{2\left(1-\frac{1}{\omega_{e1}}\right)}} \\ \|\tilde{\boldsymbol{x}}_4\| &\le \frac{1}{\omega_{e1}^{1/2}}\sqrt{\frac{\delta_{\varepsilon 1}}{2\left(1-\frac{1}{\omega_{e1}}\right)}} \end{aligned} \tag{49}$$

From (49), it is obvious that when the observer bandwidth ω_{e1} increases, the estimation errors $\tilde{\boldsymbol{x}}_1, \tilde{\boldsymbol{x}}_2$, and $\tilde{\boldsymbol{x}}_4$ decrease. Hence, Theorem 1 is proved.

PROOF OF THEOREM 3:

Substituting (22), (23) into (24), one obtains

$$\dot{\tilde{\boldsymbol{C}}}_t = -\boldsymbol{\Gamma}\boldsymbol{f}_3^T\boldsymbol{f}_3\tilde{\boldsymbol{C}}_t - \boldsymbol{\Gamma}\boldsymbol{f}_3^T(\tilde{\boldsymbol{f}}_2 - \boldsymbol{f}) \tag{50}$$

Applying the theory of time-varying linear system with noting that $\boldsymbol{\Gamma}\boldsymbol{f}_3^T\boldsymbol{f}_3$ is a diagonal matrix, the solution is given as

$$\tilde{\boldsymbol{C}}_t(t) = \tilde{\boldsymbol{C}}_t(0)\boldsymbol{\Phi}(t,0) + \int_0^t \boldsymbol{\Phi}(t,\tau)\boldsymbol{\Gamma}\boldsymbol{f}_3^T(\tilde{\boldsymbol{f}}_2 - \boldsymbol{f})d\tau \tag{51}$$

where $\boldsymbol{\Phi}(t,\tau) = \exp\left(-\int_\tau^t \boldsymbol{\Gamma}\boldsymbol{f}_3^T\boldsymbol{f}_3 d\omega\right)$.

When the persistently exciting condition (25) is satisfied, it is easy to state that $\tilde{\boldsymbol{C}}_t(0)\boldsymbol{\Phi}(t,0) \to 0$ when $t \to \infty$. The speed of this convergence depends on the value of $\boldsymbol{\Gamma}$. Thus, to prove Theorem 3, the second term on the right-hand side of (51) needs to be bounded.

Based on (25), the following inequality holds

$$\boldsymbol{\Phi}(t,\tau) \le \exp\left(-(t-\tau)\alpha_0\boldsymbol{I}_n\right) \tag{52}$$

Due to Assumptions 1, 2, and 3, there exists a constant $\delta_C > 0$ that satisfies

$$\left|\boldsymbol{\Gamma}\boldsymbol{f}_3^T(\tilde{\boldsymbol{f}}_2 - \boldsymbol{f})\right| \le \delta_C \tag{53}$$

From (52), (53), one obtains

$$\begin{aligned}&\int_0^t \boldsymbol{\Phi}(t,\tau)\boldsymbol{\Gamma}\boldsymbol{f}_3^T(\tilde{\boldsymbol{f}}_2 - \boldsymbol{f})d\tau \\ &\le \int_0^t \Phi(t,\tau)\left|\boldsymbol{\Gamma}\boldsymbol{f}_3^T(\tilde{\boldsymbol{f}}_2 - \boldsymbol{f})\right|d\tau \\ &\le \int_0^t \delta_C\exp\left(-(t-\tau)\alpha_0 I_n\right)d\tau \\ &= \frac{\delta_C}{\alpha_0}\left(1-\exp(-t\alpha_0 I_n\right) \le \frac{\delta_C}{\alpha_0} \end{aligned} \tag{54}$$

From (51), (54), it can be concluded that $\tilde{C}_t(t) \to \tilde{C}_t(\infty) \le \delta_C/\alpha_0$.

Even in the case that the persistently exciting condition (25) does not satisfy, i.e., $P_{1i} = P_{2i}$, from (50), one obtains

$$\begin{aligned}\dot{\tilde{C}}_{ti} &= 0 \\ \dot{\tilde{C}}_{tj} &= -\Gamma_j f_{3j}^T f_{3j} - \Gamma_j f_{3j}^T(\tilde{f}_{2j} - f_j)(j \ne i). \end{aligned} \tag{55}$$

When these situations occur, the identification does not work at i^{th} actuator but works well at the remaining actuators. However, these specific conditions happen intermittently at a single moment, when the actuation force direction is changed, not in a period. Hence, the persistently exciting condition holds most of the time and the identification performance is not affected at all.

REFERENCES

[1] H. E. Merritt, *Hydraulic Control Systems*. Hoboken, NJ, USA: Wiley, 1967.

[2] Y. Huang, J. Na, X. Wu, X. Liu, and Y. Guo, "Adaptive control of nonlinear uncertain active suspension systems with prescribed performance," *ISA Trans.*, vol. 54, pp. 55–145, Jan. 2015, doi: 10.1016/j.isatra.2014.05.025.

[3] J. N. Strohm, D. Pech, and B. Lohmann, "A proactive nonlinear disturbance compensator for the quarter car," *Int. J. Control, Autom. Syst.*, vol. 18, no. 8, pp. 2012–2026, Aug. 2020, doi: 10.1007/s12555-019-0531-5.

[4] M. Dong, C. Liu, and G. Li, "Robust fault diagnosis based on nonlinear model of hydraulic gauge control system on rolling mill," *IEEE Trans. Control Syst. Technol.*, vol. 18, no. 2, pp. 510–515, Mar. 2010, doi: 10.1109/tcst.2009.2019750.

[5] S. Ijaz, L. Yan, M. T. Hamayun, and C. Shi, "Active fault tolerant control scheme for aircraft with dissimilar redundant actuation system subject to hydraulic failure," *J. Franklin Inst.*, vol. 356, no. 3, pp. 1302–1332, Feb. 2019, doi: 10.1016/j.jfranklin.2018.11.018.

[6] L. Lu and B. Yao, "Energy-saving adaptive robust control of a hydraulic manipulator using five cartridge valves with an accumulator," *IEEE Trans. Ind. Electron.*, vol. 61, no. 12, pp. 7046–7054, Dec. 2014, doi: 10.1109/tie.2014.2314054.

[7] K.-X. Ba, G.-L. Ma, B. Yu, Z.-G. Jin, Z.-P. Huang, J.-X. Zhang, and X.-D. Kong, "A nonlinear model-based variable impedance parameters control for position-based impedance control system of hydraulic drive unit," *Int. J. Control, Autom. Syst.*, vol. 18, no. 7, pp. 1806–1817, Jul. 2020, doi: 10.1007/s12555-019-0151-0.

[8] D. T. Tran, D. X. Ba, and K. K. Ahn, "Adaptive backstepping sliding mode control for equilibrium position tracking of an electrohydraulic elastic manipulator," *IEEE Trans. Ind. Electron.*, vol. 67, no. 5, pp. 3860–3869, May 2020, doi: 10.1109/tie.2019.2918475.

[9] D.-T. Tran, H.-V.-A. Truong, and K. K. Ahn, "Adaptive backstepping sliding mode control based RBFNN for a hydraulic manipulator including actuator dynamics," *Appl. Sci.*, vol. 9, no. 6, p. 1265, Mar. 2019, doi: 10.3390/app9061265.

[10] H. V. A. Truong, D. T. Tran, X. D. To, K. K. Ahn, and M. Jin, "Adaptive fuzzy backstepping sliding mode control for a 3-DOF hydraulic manipulator with nonlinear disturbance observer for large payload variation," *Appl. Sci.*, vol. 9, no. 16, p. 3290, Aug. 2019, doi: 10.3390/app9163290.

[11] W. Shen and J. Wang, "Adaptive fuzzy sliding mode control based on pi-sigma fuzzy neutral network for hydraulic hybrid control system using new hydraulic transformer," *Int. J. Control, Autom. Syst.*, vol. 17, no. 7, pp. 1708–1716, Jul. 2019, doi: 10.1007/s12555-018-0593-9.

[12] J. Yao, Z. Jiao, D. Ma, and L. Yan, "High-accuracy tracking control of hydraulic rotary actuators with modeling uncertainties," *IEEE/ASME Trans. Mechatronics*, vol. 19, no. 2, pp. 633–641, Apr. 2014, doi: 10.1109/tmech.2013.2252360.

[13] J. Yao, Z. Jiao, and D. Ma, "Extended-state-observer-based output feedback nonlinear robust control of hydraulic systems with backstepping," *IEEE Trans. Ind. Electron.*, vol. 61, no. 11, pp. 6285–6293, Nov. 2014, doi: 10.1109/tie.2014.2304912.

[14] J. Yao, "Model-based nonlinear control of hydraulic servo systems: Challenges, developments and perspectives," *Frontiers Mech. Eng.*, vol. 13, no. 2, pp. 179–210, Jun. 2018, doi: 10.1007/s11465-018-0464-3.

[15] Z. Yao, J. Yao, and W. Sun, "Adaptive RISE control of hydraulic systems with multilayer neural-networks," *IEEE Trans. Ind. Electron.*, vol. 66, no. 11, pp. 8638–8647, Nov. 2019, doi: 10.1109/tie.2018.2886773.

[16] B. Yao, F. Bu, J. Reedy, and G. T. C. Chiu, "Adaptive robust motion control of single-rod hydraulic actuators: Theory and experiments," in *Proc. Amer. Control Conf.*, vol. 2, Jun. 1999, pp. 759–763, doi: 10.1109/ACC.1999.783142.

[17] B. Helian, Z. Chen, and B. Yao, "Precision motion control of a servomotor-pump direct-drive electrohydraulic system with a nonlinear pump flow mapping," *IEEE Trans. Ind. Electron.*, vol. 67, no. 10, pp. 8638–8648, Oct. 2020, doi: 10.1109/tie.2019.2947803.

[18] L. Lyu, Z. Chen, and B. Yao, "Development of pump and valves combined hydraulic system for both high tracking precision and high energy efficiency," *IEEE Trans. Ind. Electron.*, vol. 66, no. 9, pp. 7189–7198, Sep. 2019, doi: 10.1109/tie.2018.2875666.

[19] B. Xian, D. M. Dawson, M. S. D. Queiroz, and J. Chen, "A continuous asymptotic tracking control strategy for uncertain nonlinear systems," *IEEE Trans. Autom. Control*, vol. 49, no. 7, pp. 1206–1211, Jul. 2004, doi: 10.1109/TAC.2004.831148.

[20] D. Won, W. Kim, D. Shin, and C. C. Chung, "High-gain disturbance observer-based backstepping control with output tracking error constraint for electro-hydraulic systems," *IEEE Trans. Control Syst. Technol.*, vol. 23, no. 2, pp. 787–795, Mar. 2015, doi: 10.1109/tcst.2014.2325895.

[21] Z. Chu, C. Wu, and N. Sepehri, "Active disturbance rejection control applied to high-order systems with parametric uncertainties," *Int. J. Control, Autom. Syst.*, vol. 17, no. 6, pp. 1483–1493, Jun. 2019, doi: 10.1007/s12555-018-0509-8.

[22] S. Wang and J. Zhai, "A trajectory tracking method for wheeled mobile robots based on disturbance observer," *Int. J. Control, Autom. Syst.*, vol. 18, no. 8, pp. 2165–2169, Aug. 2020, doi: 10.1007/s12555-019-0156-8.

[23] X. Yu and J. Jiang, "A survey of fault-tolerant controllers based on safety-related issues," *Annu. Rev. Control*, vol. 40, pp. 46–57, Apr. 2015, doi: 10.1016/j.arcontrol.2015.03.004.

[24] Z. Gao, C. Cecati, and S. X. Ding, "A survey of fault diagnosis and fault-tolerant techniques—Part I: Fault diagnosis with model-based and signal-based approaches," *IEEE Trans. Ind. Electron.*, vol. 62, no. 6, pp. 3757–3767, Jun. 2015, doi: 10.1109/tie.2015.2417501.

[25] Y. Wang, W. Zhou, J. Luo, H. Yan, H. Pu, and Y. Peng, "Reliable intelligent path following control for a robotic airship against sensor faults," *IEEE/ASME Trans. Mechatronics*, vol. 24, no. 6, pp. 2572–2582, Dec. 2019, doi: 10.1109/tmech.2019.2929224.

[26] Y. Wang, B. Jiang, Z.-G. Wu, S. Xie, and Y. Peng, "Adaptive sliding mode fault-tolerant fuzzy tracking control with application to unmanned marine vehicles," *IEEE Trans. Syst., Man, Cybern. Syst.*, early access, Jan. 24, 2020, doi: 10.1109/tsmc.2020.2964808.

[27] Q.-N. Xu, K.-M. Lee, H. Zhou, and H.-Y. Yang, "Model-based fault detection and isolation scheme for a rudder servo system," *IEEE Trans. Ind. Electron.*, vol. 62, no. 4, pp. 2384–2396, Apr. 2015, doi: 10.1109/tie.2014.2361795.

[28] M. Muenchhof, M. Beck, and R. Isermann, "Fault-tolerant actuators and drives—Structures, fault detection principles and applications," *Annu. Rev. Control*, vol. 33, no. 2, pp. 136–148, Dec. 2009, doi: 10.1016/j.arcontrol.2009.08.002.

[29] A. S. Rezazadeh, H. R. Koofigar, and S. Hosseinnia, "Robust leakage detection for electro hydraulic actuators using an adaptive nonlinear observer," *Int. J. Precis. Eng. Manuf.*, vol. 15, no. 3, pp. 391–397, Mar. 2014, doi: 10.1007/s12541-014-0349-2.

[30] T. Li, T. Yang, Y. Cao, R. Xie, and X. Wang, "Disturbance-estimation based adaptive backstepping fault-tolerant synchronization control for a dual redundant hydraulic actuation system with internal leakage faults," *IEEE Access*, vol. 7, pp. 73106–73119, 2019, doi: 10.1109/access.2019.2920415.

[31] A. A. Amin and K. M. Hasan, "A review of fault tolerant control systems: Advancements and applications," *Measurement*, vol. 143, pp. 58–68, Sep. 2019, doi: 10.1016/j.measurement.2019.04.083.

[32] M. Van, S. S. Ge, and H. Ren, "Finite time fault tolerant control for robot manipulators using time delay estimation and continuous nonsingular fast terminal sliding mode control," *IEEE Trans. Cybern.*, vol. 47, no. 7, pp. 1681–1693, Jul. 2017, doi: 10.1109/TCYB.2016.2555307.

[33] J. Yao and W. Deng, "Active disturbance rejection adaptive control of hydraulic servo systems," *IEEE Trans. Ind. Electron.*, vol. 64, no. 10, pp. 8023–8032, Oct. 2017, doi: 10.1109/tie.2017.2694382.

[34] C. Wang, L. Quan, Z. Jiao, and S. Zhang, "Nonlinear adaptive control of hydraulic system with observing and compensating mismatching uncertainties," *IEEE Trans. Control Syst. Technol.*, vol. 26, no. 3, pp. 927–938, May 2018, doi: 10.1109/tcst.2017.2699166.

[35] T. X. Dinh, T. D. Thien, T. H. V. Anh, and K. K. Ahn, "Disturbance observer based finite time trajectory tracking control for a 3 DOF hydraulic manipulator including actuator dynamics," *IEEE Access*, vol. 6, pp. 36798–36809, 2018, doi: 10.1109/access.2018.2848240.

[36] D. T. Tran, M. Jin, and K. K. Ahn, "Nonlinear extended state observer based on output feedback control for a manipulator with time-varying output constraints and external disturbance," *IEEE Access*, vol. 7, pp. 156860–156870, 2019, doi: 10.1109/access.2019.2949594.
[37] J. Yao, W. Deng, and Z. Jiao, "Adaptive control of hydraulic actuators with LuGre model-based friction compensation," *IEEE Trans. Ind. Electron.*, vol. 62, no. 10, pp. 6469–6477, Oct. 2015, doi: 10.1109/tie.2015.2423660.
[38] A. Levant, "Robust exact differentiation via sliding mode technique," *Automatica*, vol. 34, no. 3, pp. 379–384, Mar. 1998, doi: 10.1016/S0005-1098(97)00209-4.
[39] A. Mohanty and B. Yao, "Indirect adaptive robust control of hydraulic manipulators with accurate parameter estimates," *IEEE Trans. Control Syst. Technol.*, vol. 19, no. 3, pp. 567–575, May 2011, doi: 10.1109/tcst.2010.2048569.
[40] C. Semini, N. G. Tsagarakis, E. Guglielmino, M. Focchi, F. Cannella, and D. G. Caldwell, "Design of HyQ—A hydraulically and electrically actuated quadruped robot," *Proc. Inst. Mech. Eng. I, J. Syst. Control Eng.*, vol. 225, no. 6, pp. 831–849, Sep. 2011, doi: 10.1177/0959651811402275.
[41] C. Semini, "HyQ—Design and development of a hydraulically actuated quadruped robot," Ph.D. dissertation, Italian Inst. Technol., Univ. Genoa, Genoa, Italy, 2010.
[42] J. Cieslak, D. Efimov, and D. Henry, "Transient management of a supervisory fault-tolerant control scheme based on dwell-time conditions," *Int. J. Adapt. Control Signal Process.*, vol. 29, no. 1, pp. 123–142, Jan. 2015, doi: 10.1002/acs.2465.
[43] D. Bustan, S. K. H. Sani, and N. Pariz, "Adaptive fault-tolerant spacecraft attitude control design with transient response control," *IEEE/ASME Trans. Mechatronics*, vol. 19, no. 4, pp. 1404–1411, Aug. 2014, doi: 10.1109/tmech.2013.2288314.
[44] S. A. Nahian, D. Q. Truong, P. Chowdhury, D. Das, and K. K. Ahn, "Modeling and fault tolerant control of an electro-hydraulic actuator," *Int. J. Precis. Eng. Manuf.*, vol. 17, no. 10, pp. 1285–1297, Oct. 2016, doi: 10.1007/s12541-016-0153-2.
[45] S. A. Nahian, T. Q. Dinh, H. V. Dao, and K. K. Ahn, "An unknown input Observer–EFIR combined estimator for electrohydraulic actuator in sensor fault-tolerant control application," *IEEE/ASME Trans. Mechatronics*, vol. 25, no. 5, pp. 2208–2219, Oct. 2020, doi: 10.1109/tmech.2020.3013609.
[46] D. Brambilla, L. M. Capisani, A. Ferrara, and P. Pisu, "Fault detection for robot manipulators via second-order sliding modes," *IEEE Trans. Ind. Electron.*, vol. 55, no. 11, pp. 3954–3963, Nov. 2008, doi: 10.1109/tie.2008.2005932.
[47] L. M. Capisani, A. Ferrara, A. F. D. Loza, and L. M. Fridman, "Manipulator fault diagnosis via higher order sliding-mode observers," *IEEE Trans. Ind. Electron.*, vol. 59, no. 10, pp. 3979–3986, Oct. 2012, doi: 10.1109/tie.2012.2189534.
[48] H. Yang and S. Yin, "Actuator and sensor fault estimation for time-delay Markov jump systems with application to wheeled mobile manipulators," *IEEE Trans. Ind. Informat.*, vol. 16, no. 5, pp. 3222–3232, May 2020, doi: 10.1109/tii.2019.2915668.

HOANG VU DAO received the B.E. degree in mechatronics from the School of Mechanical Engineering, Hanoi University of Science and Technology, Vietnam, in 2018. He is currently pursuing the Ph.D. degree in mechanical engineering with the School of Mechanical Engineering, University of Ulsan, Ulsan, South Korea.

His current research interests include hydraulic robots, nonlinear control, and fault tolerant control.

DUC THIEN TRAN (Member, IEEE) received the B.S. and M.S. degrees from the Department of Electrical Engineering, Ho Chi Minh City University of Technology, Vietnam, in 2010 and 2013, respectively, and the Ph.D. degree from the University of Ulsan, in 2020.

He currently works as a Lecturer with the Department of Automatic Control, Ho Chi Minh City University of Technology and Education (HCMUTE), Vietnam. His research interests include robotics, variable stiffness systems, fluid power control, disturbance observer, nonlinear control, adaptive control, and intelligent technique.

KYOUNG KWAN AHN (Senior Member, IEEE) received the B.S. degree from the Department of Mechanical Engineering, Seoul National University, in 1990, the M.Sc. degree in mechanical engineering from the Korea Advanced Institute of Science and Technology (KAIST), in 1992, and the Ph.D. degree from the Tokyo Institute of Technology, in 1999.

Since 2000, he has been with the School of Mechanical Engineering, University of Ulsan, where he is currently a Professor and the Director of the Fluid Power Control and Machine Intelligence Laboratory. He is the author or coauthor of over 190 SCI (E) papers and four books in these areas. His main research interests include fluid-based triboelectric nano generator, modeling and control of fluid power systems, energy saving construction machine, hydraulic robot, and power transmission in the ocean energy.

Dr. Ahn serves as an Editor for the *International Journal of Control, Automation and Systems*. He serves as an Editorial Board of renewable energy, Korean fluid power and construction machine, actuators, and so on.